Experimental and Numerical Design Optimization for the Geometrical Parameters Affecting Jet-pump Performance

Ahmed.M.Diab[1], Ahmed.S.Huzayyin[1] and Hesham.M.El-Batsh[1,2]
[1]Mechanical Engineering Dept, Benha Faculty of Engineering, Benha University, Egypt.
[2]Currently Professor and Dean of Higher Institute of Engineering and Technology at Mahala El-Kobra, Egypt
Email: ahmed.deyab@bhit.bu.edu.eg

Abstract:

The jet-pump is a device used for the entraining of a suction flow using a high-energy motive jet. The objective of jet-pump is achieved by three main parts: jet-nozzle, mixing chamber and diffuser. The jet-pump performance is governed by geometrical parameters that shape these parts. In this study, the most crucial geometrical parameters that influence performance are investigated by an experimental and numerical parametric study, these parameters are mixing chamber relative length (L_r), motive nozzle relative spacing (S) and area ratio between the mixing chamber and the jet orifice (A_r). Besides the parametric study, the experimental work also provides the necessary data used to validate the numerical approach, which is concluded using 2-D simulation with transition Shear-Stress Transport (SST) as a turbulence model after showing very good agreement with the experimental data. Eventually, numerical simulation is used to perform design optimization to specify the design that attains the optimum performance by Implementation the design of experiments (DOE). According to the parametric study, it is found that area ratio has the most significant impact on the jet-pump performance and operating conditions, and the highest maximum efficiency of 35.8 % is obtained at pressure ratio of 0.28 and mass ratio of 1.25 for $A_r = 4$ using L_r of 7.3 and S of 0.785. While the optimum performance is found to be within optimum mass ratio range of (2.25 - 2.96) and maximum efficiency range of (32.5 - 29.4)%.

Keywords: Jet-pump, Numerical simulation, Geometrical parameters, Flow recirculation, Design optimization, Design of experiments.

1. Introduction:

A jet-pump is a device consists of non-moving parts that is using a high energy motive jet to entrain a suction flow. Even though its efficiency is low, the jet-pump is being used in many fields for different purposes because of the simple construction and easy operation. Since its performance is already poor, it is essential to assure that the jet-pump is optimally designed. First, it is necessary to identify the geometrical parameters that have a significant impact on the performance of the jet-pump and control its design. Then a parametric study and design optimization are carried out to determine the appropriate values to be used according to the operating requirements to achieve maximum efficiency and to specify the optimum values that attain the optimum jet-pump performance. These steps may be accomplished with the aid of numerical simulation, which allows for countless test repetitions with minimal effort, time, and capability when compared to the experimental technique.

The design and geometrical characteristics of jet pumps that determine their performance have been the concern of several studies. Among these studies, Aissa [1] who used both numerical and analytical methods to examine the effects of various geometrical parameters on jet pump performance. Analytical results from MATLAB software were in good agreement with the numerical results from CFD code. At a motive flow pressure of 2.5 bar, the optimal efficiency is reached with the following parameters: area ratio (A_r) = 5.26, motive nozzle relative spacing (S) = 1, mixing chamber relative length (L_r) =

9.69 and diffuser angle = 5°. According to research conducted by Neto [2] a dimensionless formula was derived to characterize the maximum suction lift as a function of area ratio, as it was revealed that A_r played a significant role in describing the maximum suction lift of water jet-pump. In addition, researchers found that Ar was the single most influential geometrical element in determining water jet pump efficiency and cavitation limit. In the study of Sheha et al. [3], 2-D numerical simulation using transition Shear-Stress Transport (SST) turbulence model was conducted for flow simulation through jet-pump. The numerical results showed that jet pump efficiency increases with decreasing both diffuser angles and mixing chamber length up to a certain value and then efficiency decreases. Also, jet pump efficiency increases with increasing pump area ratio up to a certain value then decreases. It was found that maximum numerical efficiency is 37.8 % for A_r of 3.69. In addition, the numerical results showed that the values of L_r and diffuser angle at which peak efficiency is achieved are 5.48 5°, respectively. The study of Aldaş and Yapıcı [4] compared between 3-D numerical simulation using different turbulence models and experimental data, and it is found that the Transition SST turbulence model obtained the best result relative to experimental results among all other models. The effects of parameters such as A_r, S, and L_r on the pump performance were numerically investigated. They concluded that the maximum numerical efficiency is found to be 34.6% at A_r of 4.61, Lr of 7.4 and S 0f 0.74 at pressure ratio of 0.277. Mallela

and Chatterjee [5] who performed numerical investigation on the performance of jet-pumps. They found that incomplete mixing between the two motive and suction streams before the diffuser and the recirculation region near the mixing chamber entrance are the most important reasons for major losses in jet-pump. Also A_r is found to have a major impact on performance and the recirculation region, the best efficiency was being achieved at A_r of 3.57, Lr ranges between 7 to 9 and S ranges from 1.54 to 2.02. Halawa et al. [6] experimentally investigated some of important operational and geometrical parameters on jet pump performance. The results showed that the highest efficiency obtained was corresponding to the following jet pump configuration; $A_r = 4$, S = 1, Lr = 7.25 and diffuser angle (θ_{dif}) = 5.5° when motive flow driving pressure equals one bar. Chen [7] investigated the effect of motive nozzle angle on the jet pump performance using numerical techniques. They found that pump efficiency decreases with increasing motive nozzle angle as a result of increasing the pressure in the suction chamber and cavitation may occur if the angle is too small. Narabayashi et al. [8] examined a water jet pump experimentally and numerically using the standard k-e turbulence model, the results showed that a peak efficiency of 36% was reached at a mass ratio of 1.3 at A_r = 4. In the study of X. Long et al. [9] the influence of jet-nozzle tip design on the performance of jet pumps was investigated using CFD techniques with the standard k-e turbulence model. Optimum efficiency was found to be 34.9% at a mass ratio of 2 with $A_r = 6.27$ and jet-nozzle tip thickness of 0.2 mm. Meakhail and Teaima [10] showed that the motive nozzle relative spacing should be 0.5 for maximum jet-pump efficiency, and the liquid jet pump is significantly prone to cavitation as motive nozzle relative spacing is reduced to zero.

Such as other pump types, there are losses associated with the flow field of the jet-pump, and as outlined by Cunningham [11], the potential major losses through jet-pumps are the mixing loss, which is maximum at low mass ratios when the relative velocity between the motive and suction flows is a maximum and decreases as the mass ratio increases and this loss is related to the formation of flow recirculation, another major loss is the friction loss that greatly increases with mass ratio and with high velocities. Flow recirculation, which is one of the most energy losses phenomena that the flow through jet-pump is characterized with, was the concern of many studies that investigated the flow through jet-pumps such as Elger et al. [12], Ryzhenkov et al. [13], Antoine et al. [14], X. Long et al. [9] and Xiao et al. [15]. The latter study investigated the influence of A_r on the formation of recirculation region in jet-pumps, the study was based on 2-D axisymmetric numerical modelling using RNG k-ϵ as a turbulence model. The results showed that A_r has significant impact on the size and location of recirculation, and the formation of recirculation is due to

the high velocity difference between the motive and suction flows.

Literature reviews have identified four geometrical parameters, mixing chamber relative length, motive nozzle relative spacing, diffuser angle and area ratio, as having the largest effect on jet-pump performance. While there is consensus that the diffuser angle that attains the maximum efficiency lies between 5 and 5.5°, the values of the other parameters vary. As a result, the aim of this study is to initially conduct a parametric study for mixing chamber relative length (L_r), motive nozzle relative spacing (S) and area ratio (A_r) to find out how these parameters can affect the jet pump and to specify the values that achieves the maximum jet pump efficiency. Following that, a design optimization is performed to specify the geometrical parameters values based on achieving the optimum performance. The parametric study will be conducted by experimental work and 2-D numerical simulation as it has been demonstrated that the flow behavior through jet-pump can be successfully simulated using numerical methods. The transition SST model will be adopted in the present numerical study as the previous studies obtained good numerical predictions for the experimentally measured data using this model. However, A model validation test is held by comparing the 2-D simulation results with the experimental results under the same geometrical and operational conditions.

2. Methodology
2.1 Jet-pump model

The model of jet-pump used in experimental work and numerical simulation is shown in fig. 1, the dimensions of jet pump model are listed in table 1.
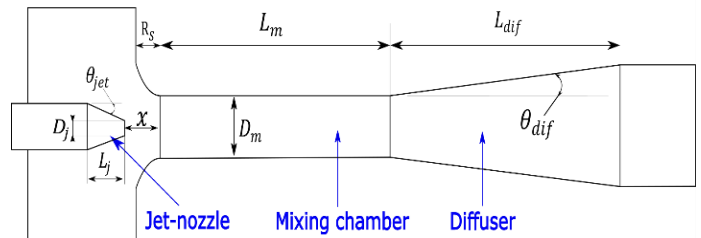

Fig (1) Schematic of jet-pump model.

Table (1) Jet-pump model dimensions.

D_m (mm)	D_j (mm)	L_m (mm)	L_j (mm)	R_s (mm)	L_{dif} (mm)	θ_{jet} (°)	θ_{dif} (°)
35	16.3	259	60	25	218	16	5.5

The present study will be restricted to investigate the effect of the following geometrical parameters:

1- Motive nozzle relative spacing (S), defined as the ratio of the axial distance between jet-nozzle orifice and mixing chamber inlet to the mixing chamber diameter:
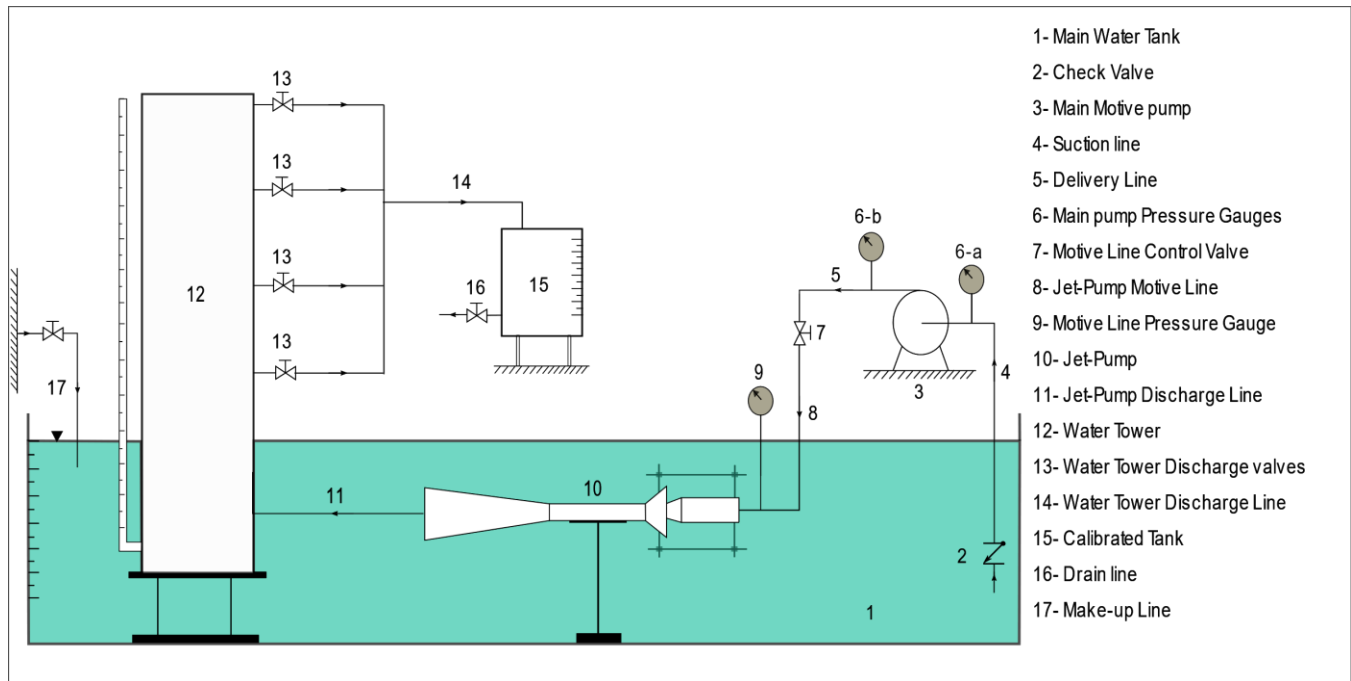
Fig. (2) Schematic diagram of experimental set-up.

$$S = \frac{x}{D_m} \qquad (1)$$

2- Mixing chamber relative length (L_r), defined as the ratio between the mixing chamber length and the mixing chamber diameter:

$$L_r = \frac{L_m}{D_m} \qquad (2)$$

3- Area ratio (A_r), defined as the ratio between the mixing chamber area and the jet-nozzle orifice area:

$$A_r = \frac{A_m}{A_j} = \left(\frac{D_m}{D_j}\right)^2 \qquad (3)$$

2.2 Experimental test rig

The experimental work is used to investigate the effect of motive nozzle relative spacing (S) on the performance of jet-pumps and to provide the data that is used to validate the numerical simulation. The experimental work is achieved by constructing a test rig including jet-pump model in the fluid mechanics laboratory of the mechanical power engineering department, faculty of engineering, Benha university, Egypt. The jet-pump model is 3-D printed from Polylactic Acid (PLA) plastic material. The experimental set-up is shown in fig. 2.

The test rig is designed in a manner that enables changing motive nozzle relative spacing of jet pump (S), which is modified by adjusting the axial distance between the jet-nozzle orifice and the mixing chamber inlet to obtain four S of 0.5, 0.75, 1 and 1.25. The main tank (1) is filled with water and kept at constant level throughout the run using a make-up line (17) to maintain a constant suction head for the centrifugal pump (3) and to keep the suction flow head (P_s) for the jet pump (10) constant at a

value of 0.2 mH2o. The motive flow rate ($\dot{m}_p$) is adjusted at 2 kg/s for all runs using the motive line control valve (7), then the motive pressure is measured by the motive line pressure gauge (9). The jet pump discharge head is adjusted at different levels by allowing the water to discharge through the water tower discharge valves (13) installed at different levels above the jet pump discharge pipe, the jet-pump discharge head (P_d) is set to 0.6, 1, 1.4 and 1.8 mH2O. At each opening valve the corresponding discharge flow rate is calculated by measuring the time required to fill known volume calibrated tank (15) using a timer.

Uncertainty analysis should be conducted on all data collected from all measurements in order to quantify the data and validate the accuracy. The estimation of the uncertainty intervals is taken as one-tenth of the scale division of the instrument [16]. The quantities measured directly in the experiment include static head by a ruler measure, static pressure by a pressure gauge, and flow rate by calibrated tank and stop watch. The uncertainties in measuring these quantities were evaluated to be $\pm$0.1 mm, $\pm$0.002 bar and $\pm$0.1 second, respectively
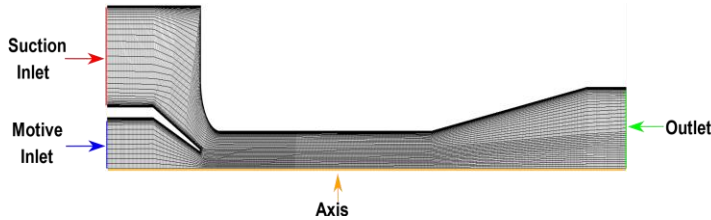
2.3 Numerical simulation:

Numerical simulation is used to investigate the effect of the geometrical parameters on the performance of jet-pumps and to perform the design optimization. Numerical calculations are performed using the commercial CFD package Ansys Workbench version 18.2. The numerical study is based on axisymmetric 2-D numerical simulation as the cylindrical symmetric jet-pump construction and the absence of the tangential flow component enable

using this approach without losing any physical insight of the operating of the jet pump.

2.3.1 Computational domain and grid generation

The Computational domain of 2-D jet pump model is generated using Design Modeler software. Figure 3 illustrates the computational domain with the selected boundaries of jet-pump. Then, a high-quality structural mesh is produced using ICEM software with mesh Inflation near the wall boundaries to improve accuracy in the boundary layer simulation and concentrated mesh in the region of suction nozzle and the beginning of the mixing chamber as can be seen in the mesh details in fig. 3.

Fig. (3) The computational domain and mesh details of jet-pump model.

2.3.2 Solver

- **Governing equations**

The numerical simulation is undertaken based on two-dimensional, steady, single-phase flow of water, which is incompressible, viscous and Newtonian fluid, with no heat transfer between water and surroundings through the jet pump. Based on these assumptions, the governing equations are the Reynolds Averaged Navier-Stokes (RANS) continuity and momentum equations [17].

- **Turbulence model**

For the closure of the governing equations and the turbulence flow modelling, the transition Shear-Stress Transport (SST) turbulence model has been used, which is based on the coupling of the SST k-ω transport equations with two other transport equations, one for the intermittency and one for the transition onset criteria, in terms of momentum-thickness Reynolds number [18].

The two transport equations for SST $k - \omega$ model to obtain the turbulence kinetic energy (k) and the specific dissipation rate (ω) are as follows:

$$\frac{\partial}{\partial t}(\rho k) + \frac{\partial}{\partial x_i}(\rho k u_i) = \frac{\partial}{\partial x_j}\left(\Gamma_k \frac{\partial k}{\partial x_j}\right) + \widetilde{G_k} - Y_k + S_k \quad (4)$$

$$\frac{\partial}{\partial t}(\rho \omega) + \frac{\partial}{\partial x_i}(\rho \omega u_i) = \frac{\partial}{\partial x_j}\left(\Gamma_\omega \frac{\partial \omega}{\partial x_j}\right) + G_\omega - Y_\omega + D_\omega + S_\omega \quad (5)$$

Where; $\widetilde{G_k}$ is the production of turbulence kinetic energy due to velocity mean gradient

G_ω is the generation of ω

Γ_k and Γ_ω are the effective diffusivity of k and ω, respectively.

Y_k and Y_ω are the dissipation of k and ω due to turbulence.

D_ω is the cross-diffusion term.

S_k and S_ω are source terms defined by the users.

The transport equation for the intermittency γ, which is a measure of the probability that a given point is located inside the turbulent region, is defined as:

$$\frac{\partial(\rho\gamma)}{\partial t} + \frac{\partial(\rho U_j \gamma)}{\partial x_j} = P_{\gamma 1} - E_{\gamma 1} + P_{\gamma 2} - E_{\gamma 2} +$$
$$\frac{\partial}{\partial x_j}\left[\left(\mu + \frac{\mu_t}{\sigma_\gamma}\right)\frac{\partial\gamma}{\partial x_j}\right] \quad (6)$$

Where; $P_{\gamma 1}$ and $E_{\gamma 1}$ are the transition sources.

$P_{\gamma 2}$ and $E_{\gamma 2}$ are the destruction sources.

σ_γ is a constant

At last, the transport equation for the transition momentum thickness Reynolds number $\widetilde{Re_{\theta t}}$, which indicated the transition onset criteria, is:

$$\frac{\partial(\rho\widetilde{Re_{\theta t}})}{\partial t} + \frac{\partial(\rho U_j \widetilde{Re_{\theta t}})}{\partial x_j} = P_{\theta t} + \frac{\partial}{\partial x_j}\left[\sigma_{\theta t}(\mu + \mu_t)\frac{\partial\widetilde{Re_{\theta t}}}{\partial x_j}\right] \quad (7)$$

Further details regarding the transition SST model are given by Menter et al. [19] and Langtry et al. [20]

- **Solver setup**

The numerical resolution of the governing equations is performed by adopting Ansys Fluent, which is a finite volume-based program. The 2D double-precision pressure-based solver type was selected for a better resolution of the turbulent flow field. A coupled algorithm was applied to solve the coupling of the pressure and velocity, with using a second-order scheme for pressure and momentum to solve the flow field, The result is obtained for a steady state flow. The residual for convergence criteria is taken less than 10^{-4}, and iterations are continued until the convergence is satisfied.

- **boundary conditions**

Boundary conditions are set as follows. The inlet boundaries, consisting of the motive flow inlet is settled as uniform mass-flow-inlet, and the suction flow inlet is settled as total-pressure-inlet, while the outlet boundary is designed as static-pressure-outlet. Boundary condition in the wall was treated as non-slip wall condition, and the boundary type of axis of the jet-pump, corresponding to 2D case, is set as symmetric boundary. In the calculations for the present study, the motive mass flow $(\dot{m}_p)$ and total pressure for suction flow $(P_{t.s})$ are kept fixed at 2 kg/s and 0.2 mH$_2$O, respectively, and the outlet static pressure varies to obtain the full operating range of the tested model.

3. Results and discussion
3.1 Model validation

The data obtained from experimental measurements and numerical calculations are used to determine dimensionless performance parameters, which characterize and express jet pump performance and operating conditions, these parameters are defined as follows:

1- Mass ratio (M_r): the ratio of suction flow rate to the motive flow rate:

$$M_r = \frac{\dot{m}_s}{\dot{m}_p} \quad (8)$$

2- Pressure ratio (P_r): the ratio of the increase in suction flow total pressure to the decrease in motive flow total pressure:

$$P_r = \frac{P_{t.d} - P_{t.s}}{P_{t.p} - P_{t.d}} \qquad (9)$$

3- Jet pump efficiency (η): the ratio of the suction flow energy gain to the motive flow energy loss:

$$\eta = \frac{m_s \times (P_{t.d} - P_{t.s})}{m_p \times (P_{t.p} - P_{t.d})} = M_r \times P_r \qquad (10)$$

A grid independence study was carried out to find suitable grid size required for the calculations using jet-pump efficiency as comparison criterion. The grid study is performed at $m_p = 2kg/s$, $P_{t.s} = 0.2\,mH_2o$ and $P_d = 1.4\,mH_2O$. Five different grid resolutions were used, with cells total number of 40267, 52036, 78088, 96328 and 243396. The grid independence test result is illustrated in fig. 4. Figure 4 shows that raising the total number of grids from 78088 to 234496 resulted in an efficiency divergence of just 0.37%. As a result, a grid size of 78088 cells is used, which is satisfactory in terms of accuracy and solution economy. Also, the dimensionless wall distance y+ is smaller than 1 which satisfies the calculation of the viscous sub-layer.
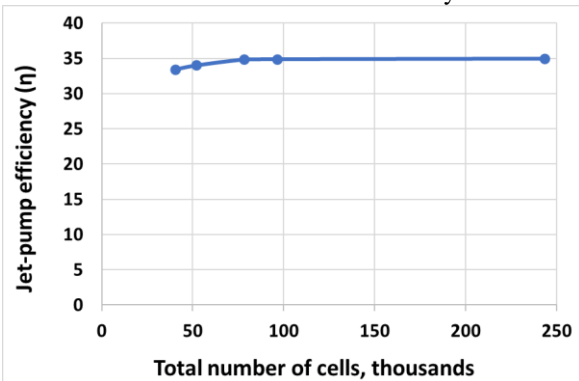

Fig. (4) Calculated efficiency at different grid resolution.

The validation of numerical simulation is based on comparing experimental dimensionless performance characteristics curves of jet pump for different motive nozzle relative spacing (S) with those of numerical approach. The comparison is performed for S = 0.5, 0.75, 1 and 1.25. Other geometrical parameters are the same as for the model in fig.1. The result of validation is illustrated in fig. 5, which shows the dependence of the pressure ratio and jet-pump efficiency on the mass ratio. The 2-D simulation results show very good agreement with the experimental measurements over entire operating range with acceptable deviation noticed between the two approaches, which is believed is due to surface roughness of the manufactured jet pump model by 3-D printing. As can be seen in fig. 5, for each S, the efficiency increases till a maximum value (η_{max}) then decreases. The highest maximum efficiency is obtained for S = 0.75, which is 35.1% achieved at M_r =1.4.

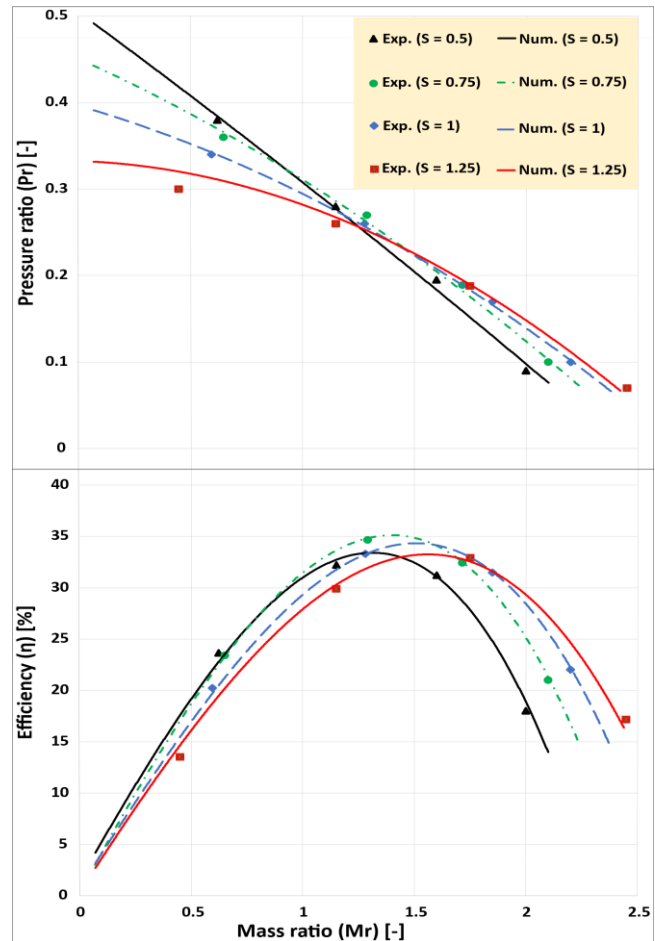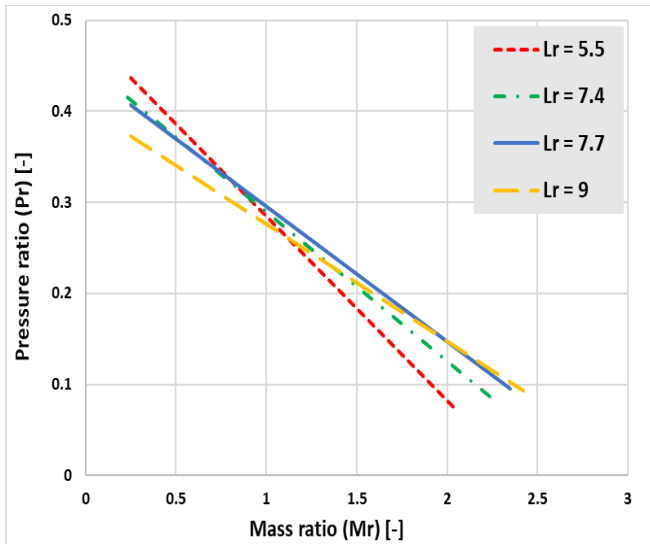**Fig. (5)** Experimental and numerical performance curves using different S.
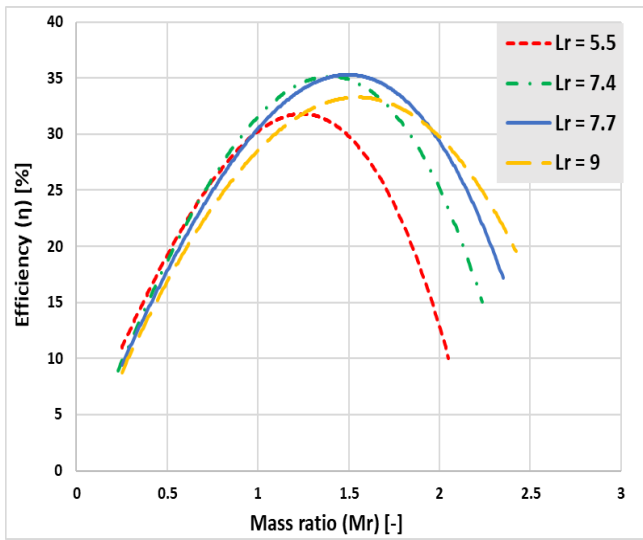
3.2 Effect of geometrical parameters:
3.2.1 Effect of mixing chamber relative length:

Four different mixing chamber lengths are used in combination with one mixing chamber diameter resulting in four mixing chamber relative lengths (L_r) of 5.5, 7.4, 7.7 and 9, this range encompasses L_r that achieves highest η_{max} found in literature, while other dimensions are the same as for the model depicted in fig. 1 with using motive nozzle relative spacing (S) equals to 0.75, which was found to achieve highest η_{max}. Figure 6 demonstrates the effect of Lr on the jet-pump performance, for each Lr the efficiency increases with M_r to a maximum value then decreases. The highest maximum efficiency of 35.3% is achieved for Lr = 7.7 at $P_r = 0.235$ by attaining $M_r = 1.5$. While the mass ratio is only 1.27 and 1.35 for Lr = 5.5 and 9, respectively, at the same P_r condition.

Figure 7 illustrates contours of dimensionless velocity (V_r) at $P_r = 0.23$, where V_r is the local flow velocity normalized by jet-nozzle downstream velocity (v_j). In case of Lr = 7.7, the mixing process and momentum transfer between the suction and motive flows completes by the end

(a)

(b)

Fig. (6) Effect of Lr on jet-pump performance.

Fig. (7) Dimensionless velocity contours at $P_r = 0.23$

Fig. (8) jet-pump centerline Cp distribution along mixing chamber (M.C.) and diffuser at $P_r = 0.23$

of the mixing chamber, where the flow is almost fully developed and has nearly uniform velocity profile. When Lr = 9, the velocity profile is almost unchanged after the distance of Lr = 7.7 as seen in fig. 7 (c). This additional distance of mixing chamber leads to friction loss and pressure reduction in the mixing chamber before pressure recovery in the diffuser. Figure 8 shows the distribution of the static pressure coefficient (Cp) along the centerline which defined as :

$$C_p = \frac{P - P_s}{\frac{1}{2}\rho v_j^2} \qquad (11),$$

where P is the local static pressure, Ps is suction static pressure, ρ is flow density and v_j is jet-nozzle downstream velocity. The pressure starts to decrease in the mixing chamber after attaining a maximum value at dimensionless length (L/Dm) = 11.85, which corresponds to the position of the mixing chamber end for Lr = 7.7. Whereas for Lr =
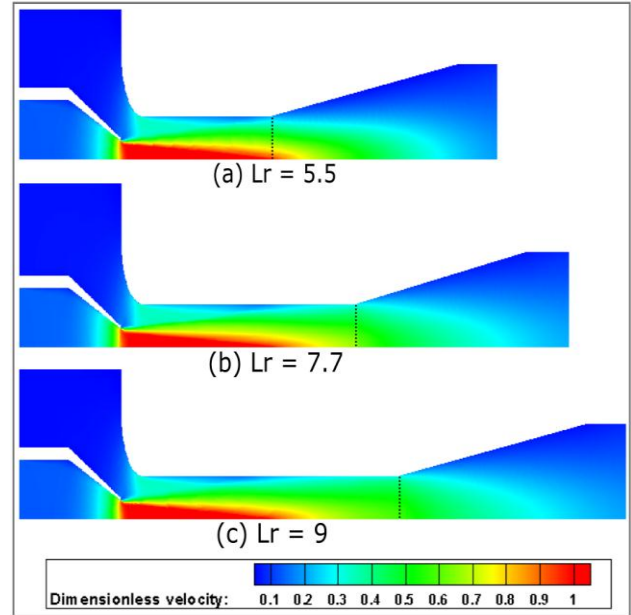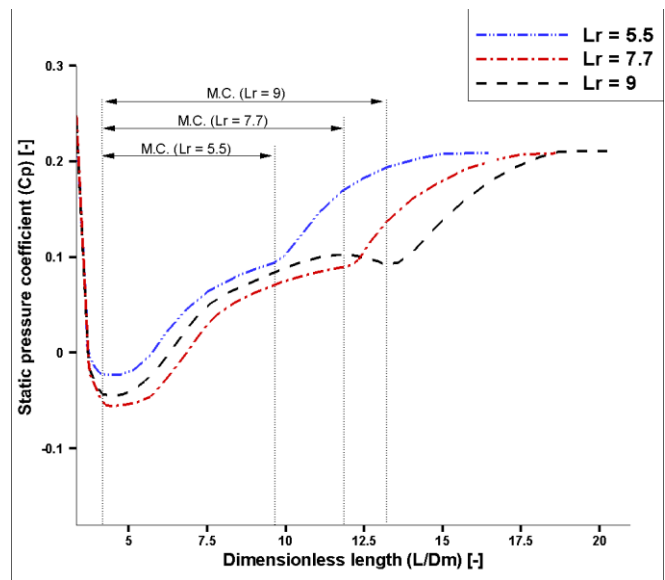
5.5, the mixing process is not accomplished by the end of the mixing chamber, which leads to discharge the flow towards the diffuser with incomplete mixing and before achieving uniform velocity profile as shown in fig. 7 (a), also the flow seems not to achieve the same pressure raising of longer L_r within the mixing chamber as seen in fig. 8. By contrast, the motive flow of Lr = 7 obtains lower pressure after the jet-nozzle as can be seen in fig. 8. When the motive flow pressure falls below the suction flow pressure ($C_p < 0$), the suction process takes place, and the lower the pressure, the more the amount of the flow that is sucked. Therefore, Lr = 7 achieves higher M_r compared to

Lr = 5.5 and 9 for the same P_r condition and obtaining higher efficiency. As P_r decreases which means

increasing mass ratio, that makes the mixing process needs longer distance to complete momentum transfer to the increased flow rate, for that as P_r decreases, Lr that attains better performance increases.

3.3.2 Effect of area ratio:

The effect of area ratio (A_r) on the performance of jet-pump is investigated by combining seven distinct mixing chamber diameters (D_m) with a single motive nozzle orifice diameter (D_j), yielding seven A_r values ranging from 3 to 12. Figure 9 depicts the numerical solutions obtained using Lr = 7.7 and S = 0.75. As can be seen, η_{max} reaches a peak value for $A_r = 4$ then gradually decreases with any increase of A_r.

(a)

(b)
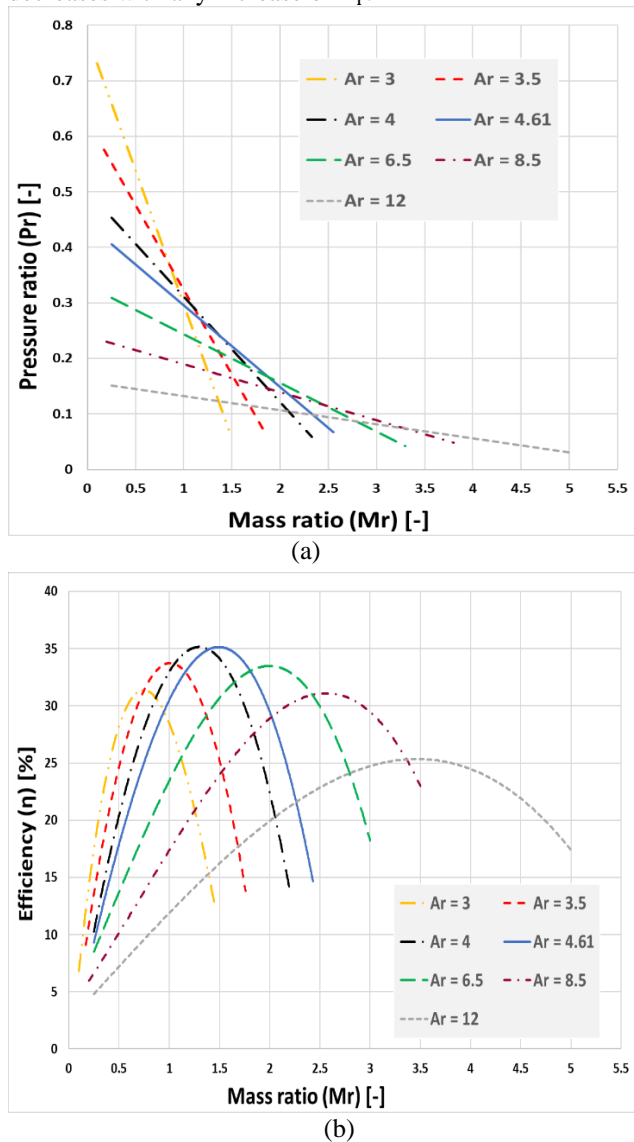
Fig. (9) Effect of area ratio A_r on jet-pump performance using S = 0.75, Lr = 7.7
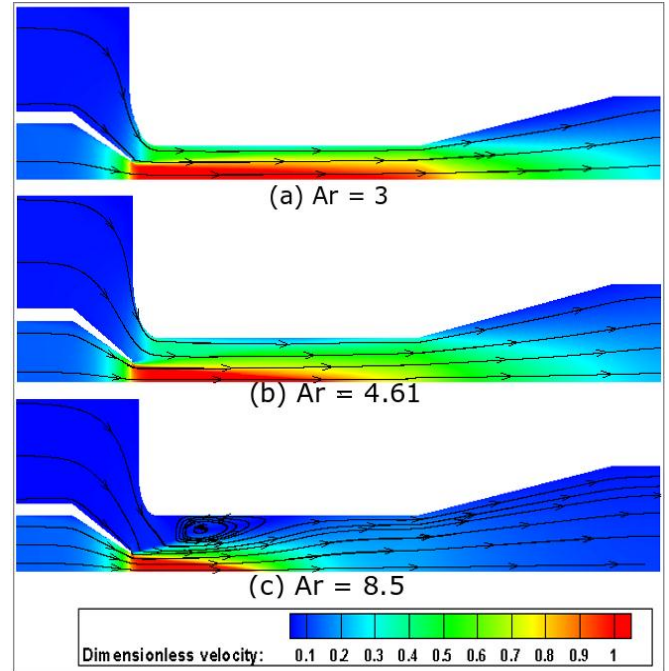
Fig. (10) Dimensionless velocity contours at $P_r = 0.2$, using S = 0.75, Lr = 7.7

A demonstratively important notice from figs. 5,6 and 9, the performance is more affected by A_r compared to S and Lr, as A_r has great impact on the mass ratio of the jet-pump. Using $A_r = 6.5$ instead of 4 would increase M_r of η_{max} by 40% while the drop in η_{max} is just 5.7%, on the contrary, increasing S from 0.75 to 1.25 would increase M_r of η_{max} by 10.2%, while η_{max} drops by approximately 7.5%. So, the loss in η_{max} is justified by the advantage of mass ratio increase in case of changing A_r, while for S and Lr, the gain in M_r doesn't compensate for the performance loss. To understand how A_r greatly affects the performance, the flow field is obtained for A_r = 3, 4.61 and 8.5 at $P_r = 0.2$. At this P_r, highest efficiency is achieved using $A_r = 4.61$ at $M_r = 1.65$, while M_r for A_r = 3 and 8.5 for the same output pressure are just only 1.2 and 0.8, respectively. As can be seen in fig. 10 (a), which shows the contours of V_r, the flow velocity in the mixing chamber of $A_r = 3$ is higher than other A_r models, and there is a negative total pressure coefficient region besides the mixing chamber wall as can be seen in fig. 11 (a), which illustrates total pressure coefficient (C_{p-t}) defined as:

$$C_{p-t} = \frac{P_t - P_{t.s}}{\frac{1}{2}\rho_w v_j^2}$$ (12),

where P_t is the local total pressure, $P_{t.s}$ is suction total pressure. Negative C_{p-t} region refers to total pressure loss due to the high fluid friction near the wall for low A_r that results in flow rate reduction.

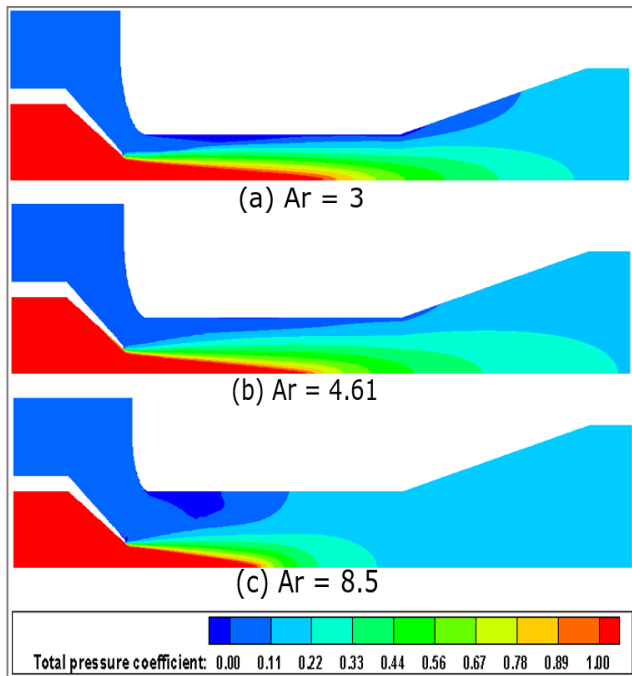While for $A_r = 8.5$, the suction flow velocity is too low relative to the motive flow due to the large annular area

Fig. (11) Total pressure coefficient contours at $P_r = 0.2$, using S = 0.75, Lr = 7.7

Fig. (12) Dimensionless velocity contours at $P_r = 0.1$

which causes flow recirculation region near the wall of the mixing chamber on the suction flow side [9] as can be seen in fig. 10 (c), this phenomenon affects the suction duty of the jet-pump, as part of the suction flow gets recirculated which leads to flow rate reduction. It is obvious that the region of total pressure loss in fig. 11 (c) is compatible with the region of recirculation in fig. 10 (c). All that makes the motive momentum being rapidly dissipated without sufficient momentum transfer to the suction flow, and the flow exits the mixing chamber with low velocity. On the contrary, in case of $A_r = 4.61$, the flow avoids the losses due to either the friction or the formation of flow recirculation as seen in fig. 11 (b), so more flow can be delivered for the same Pr. As P_r decreases the velocity through mixing chamber increases due to the increased flow rate as can be seen in fig. 12, which illustrates dimensionless velocity at $P_r = 0.1$, which causes greater friction losses for small A_r, while recirculation region size gets decreased for large A_r as the suction flow velocity increases, for that the recirculation region vanishes for $A_r = 8.5$ at $P_r = 0.1$ as shown in fig. 12 (c), that is way as P_r decreases, A_r at which η_{max} obtained increases as illustrated in fig. 9.

A_r directly affects the major losses causes through the flow field outlined by Cunningham [11], making it the most essential geometrical parameter that controls performance of jet-pump, and first parameter that must be taken into consideration throughout the jet-pump design process.
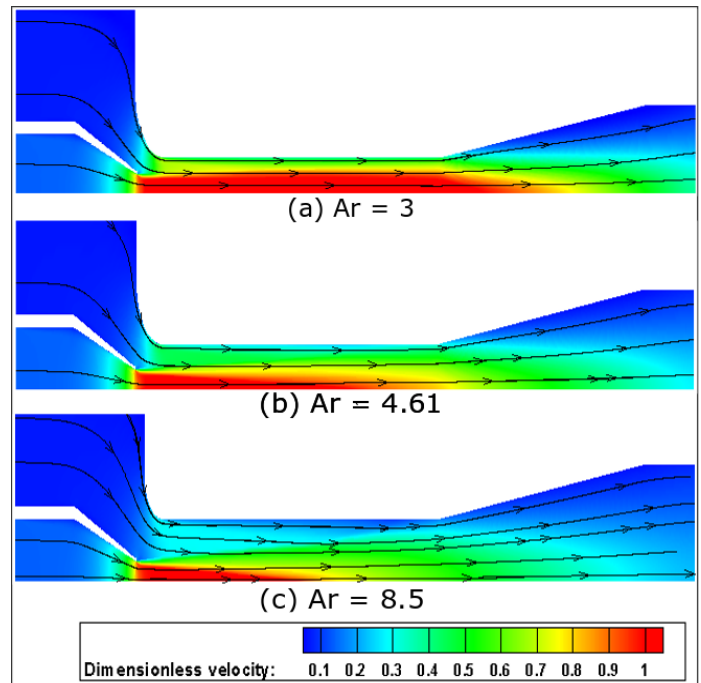
3.4 Jet-pump maximum efficiency design criteria:

First step of jet-pump design based on maximum efficiency criteria is to determine the appropriate area ratio (A_r) according to the operating requirements, for that area ratio selection curve is plotted in fig. 13 by making use of the data in fig. 9. Figure 13 illustrates A_r that should be utilized for each pressure ratio (P_r) as it provides the maximum efficiency (η_{max}) at this P_r. If other A_r is arbitrarily used, the pump may operate with a lower efficiency. Second step is the appropriate geometrical parameters selection, which is established based on the results of numerical calculations for variety values of motive nozzle relative spacing (S) and mixing chamber relative length (L_r) at different A_r. Figure 14 shows the appropriate values of S and L_r that achieve the highest maximum efficiency for each A_r.
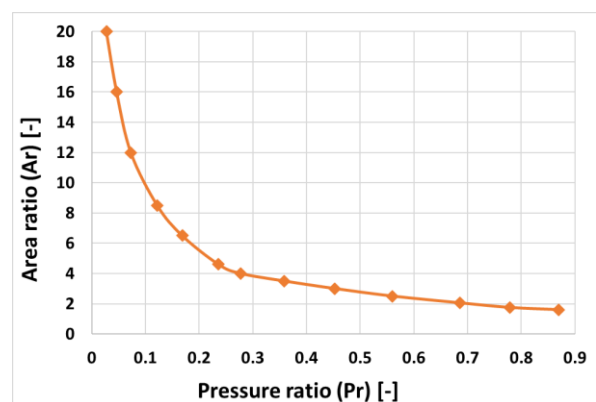

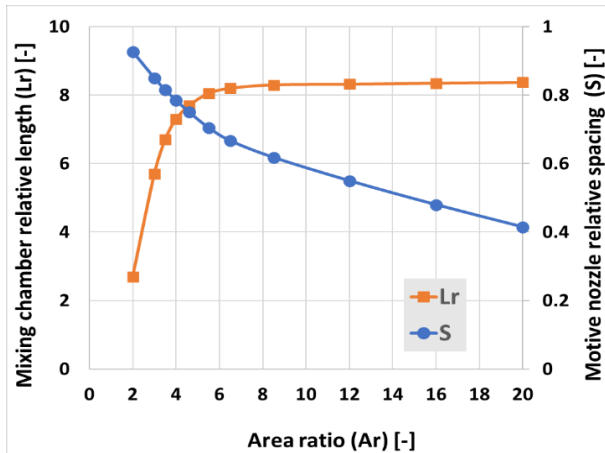**Fig. (13)** Appropriate A_r selection curve

Fig. (14) Appropriate selection of geometrical parameters

As shown in the fig, S always tends to decrease with the increase of A_r. While L_r sharply rises up to around A_r = 6.5, then remains constant at approximately value of 8.4. The correlation between the three parameters is related to the mixing process between the motive and suction streams. The appropriate selection of Lr and S for a certain A_r guarantees the completing of mixing process and momentum transfer by the end of the mixing chamber, allowing these selected values to achieve the highest performance compared to other values of S and Lr. As the momentum transfer occurs, the velocity difference between the motive and the suction flows decreases till the uniform velocity profile is reached. The distance required by the flow to complete the mixing process is directly proportional to the initial velocity difference between the two streams at the beginning of the mixing process. Figure 15, illustrates the dimensionless velocity for the suction flow side ($V_{r.s}$) at the entrance of the mixing chamber where the mixing process is just at the beginning. $V_{r.s}$ is numerically determined for each Ar at the corresponding P_r in fig. 13. As can be seen, $V_{r.s}$ decreases sharply as A_r increases which means the initial velocity difference between the two streams increases so mixing process needs longer distance to complete, that is why appropriate L_r
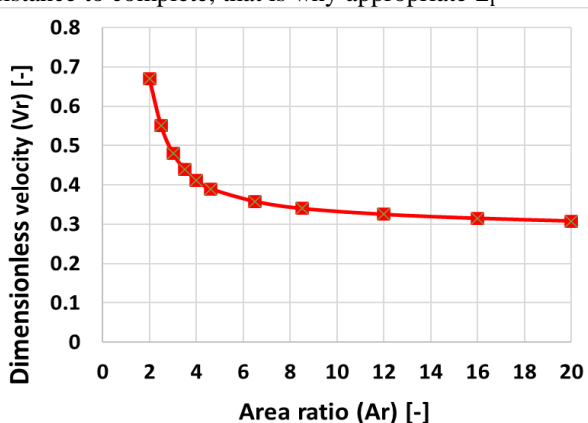

Fig. (15) Suction flow dimensionless velocity ($V_{r.s}$) at mixing chamber inlet for the conditions of η_{max}.
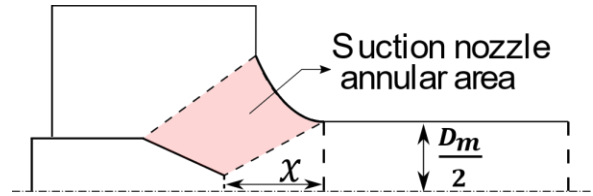

Fig. (16) Suction nozzle annular area

increases as A_r increases. When A_r exceeds 6.5, $V_{r.s}$ hardly changes, so the mixing process requires almost the same distance to complete, as a result, L_r keeps constant after A_r = 6.5. The effect of changing S is somehow similar to changing A_r, where both affect the suction nozzle annular area illustrated in fig. 16. So as A_r increases the corresponding S decreases trying to eliminate the effect of A_r.

The maximum efficiencies and the corresponding M_r conditions are numerically calculated using the appropriate L_r and S for each A_r and plotted in fig. 17. According to the curves of fig. 17, the highest η_{max} achieved is 35.8 % and the corresponding M_r is 1.25 obtained at P_r = 0.28 for A_r = 4 using Lr = 7.3 and S = 0.785. Also, from the figure it can be concluded that η_{max} becomes zero when A_r is 1.4 as M_r becomes zero, which means using $A_r \leq 1.4$ makes jet-pump unable to perform the suction duty which is its main goal. However, it is strongly recommended to avoid using A_r values lower than 2, as the achievable η_{max} decreases significantly. When A_r is reduced from 3 to 2, the highest η_{max} drops from 33.8% to around 25.5%, if A_r is further decreased to 1.5, the highest maximum efficiency plummets to only 7%. In addition, it is not recommended to use $A_r > 14$ unless high Mr is required, as the highest η_{max} drops below 25 % for.
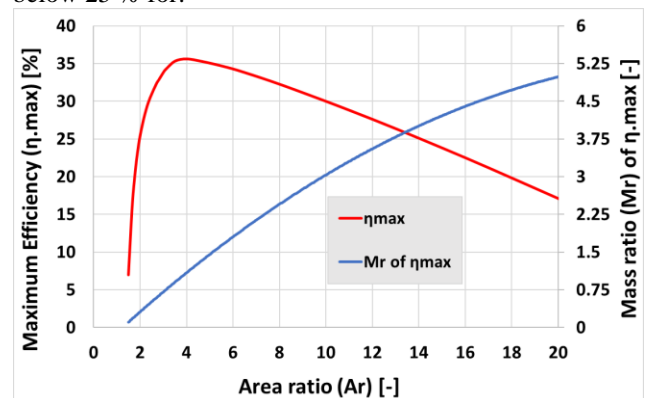
Fig. (17) Curves of maximum efficiency conditions.

3.5 Design optimization:

The goal of a jet pump is entraining a suction flow, and delivering as much flow as possible with attaining the highest feasible efficiency to achieve high output pressure, so attaining the condition of highest maximum efficiency doesn't satisfy the optimum performance criteria, which should take both maximum efficiency and mass ratio into consideration. The optimum design of geometrical

parameters that satisfies the optimum performance criteria is obtained by an optimization technique, which is performed using Response Surface Optimization (RSM) feature impeded in Ansys package. The first step of the optimization is to set the Design of Experiment (DOE) [18]. The geometrical parameters; A_r, Lr and S are set as input parameters, while η_{max} and M_r are set as output parameters. A Latin Hypercube Sampling Design (LHSD) method [21, 22] is used to set the samples in the DOE. In the current study, area ratio (A_r) is varied from 2 to 14. The mixing chamber relative length (Lr) is set between 5 and 9.5. The motive nozzle relative spacing (S) is set between 0.25 and 1.5. This allows for testing a wide variety of values widening the optimization selection range. The Kriging method, which is a stochastic interpolation method [23, 24], is used to interpolate the data of the DOE during the RSM. To improve the accuracy of Kriging method, large number of the samples must be used. So, the number of samples used in this study is 40. The optimization step is carried out using Multi-Objective Genetic Algorithm (MOGA) which supports all types of input parameters. The optimization objective is set as maximum η_{max} and maximum M_r. The optimization is performed on three stages with three candidate designs for each stage. The candidate designs are numerically investigated using Fluent to check the validation of optimization, the numerically calculated η_{max} and M_r are compared to the optimization expected values to calculate the error, this data is provided again to

the optimization tool to be used to specify new stage of candidate designs. The average stage error gets decreased till it becomes less than 1 % for both η_{max} and M_r at the third stage as can be seen in fig. 18, so the designs of third stage are considered the optimum designs.
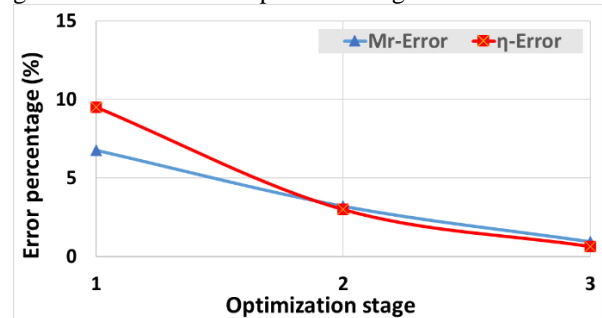

Fig. 18: Average error sensitive curve.

The three optimum designs of the third stage are tabulated in table 2, in addition, the design that attains the highest η_{max} is listed. As can be noticed the optimum operating M_r range is from 2.25 to around 3 with attaining optimum η_{max} range from 29.4 to 32.5%. The optimum η_{max} range doesn't include the highest η_{max}, as M_r of the highest η_{max} is relatively low as can be seen in the table.

Using the optimum designs results in the reduction of η_{max} by (9.2 - 17.9)% relative to the highest η_{max}, while the increase in M_r is about (80 -136.8)%, making the usage of these optimum ranges justified.

Table 2: Optimization designs, and the design based on η_{max}					
Optimum design	A_r	L_r	S	η_{max}	M_r
1	6.875	9.0716	0.67	32.5	2.25
2	7.755	9.436	1.37	30.2	2.85
3	9.035	9.4539	0.712	29.4	2.96
Design based on η_{max} criteria	4	7.3	0.785	35.8	1.25

Conclusions

A parametric study is carried out experimentally and numerically for the most three important geometrical parameters affecting jet-pump performance; mixing chamber relative length, motive nozzle relative spacing and area ratio. The numerical approach, which is concluded based on 2-D simulation using transition SST turbulence model, achieves good agreement with the experimental results with very small deviation between the numerical and experimental efficiencies due to surface roughness of the 3-D printed experimental model. The results of parametric study showed that A_r is the most dominant factor controlling the performance and operating mass ratio of jet-pump, as it has great impact on the formation of flow recirculation through

jet-pump and the friction forces besides the wall of mixing chamber. The efficiency of jet-pump increases with A_r till highest η_{max} of 35.8 % is obtained at P_r = 0.28 and M_r = 1.25 for A_r = 4 using L_r = 7.3 and S = 0.785, with the increase of A_r, η_{max} starts to decrease. It is recommended to use A_r within the range $2 > A_r > 14$, otherwise the achievable maximum efficiency drops below 25%. A design optimization is performed to specify the jet-pump designs that achieve optimum performance. Three optimum designs are obtained and found to achieve an optimum performance with η_{max} range of (32.5 – 29.4)% and M_r range of (2.25 – 2.96).

Nomenclature

A_r Area ratio   [-]
C_p Static pressure coefficient   [-]
C_{p-t} Total pressure coefficient   [-]
D_j Jet-nozzle orifice diameter   [mm]
D_m Mixing chamber diameter   [mm]
L Axial position [mm]
L_m Mixing chamber length   [mm]
L_r Mixing chamber relative length   [-]
M_r Mass ratio [-]
$\dot{m}$ Mass flow rate   [kg/s]
P Static pressure [Pa]
P_r Pressure ratio   [-]
P_t Total pressure   [Pa]
S Motive nozzle relative spacing   [-]
V_r Dimensionless velocity =` local flow velocity/v_j [-]
v_j Jet-nozzle downstream velocity [m/s]
x Axial distance between jet-nozzle orifice and mixing
     chamber inlet   [mm]
η Jet-pump efficiency   [%]

Subscript

d discharge flow
j jet-nozzle orifice
m mixing chamber
p motive flow
s   suction flow

References

[1] W. A. Aissa, "Experimental and Theoretical Investigation of Water Jet Pump Performance," vol. 3, no. 1, pp. 1–13, 2021.

[2] I. E. L. Neto, "Maximum suction lift of water jet pumps," *J. Mech. Sci. Technol.*, vol. 25, no. 2, pp. 391–394, 2011.

[3] A. A. A. Sheha, M. Nasr, M. A. Hosien, and E. M. Wahba, "Computational and Experimental Study on the Water-Jet Pump Performance," vol. 11, no. 4, pp. 1013–1020, 2018, doi: 10.18869/acadpub.jafm.73.247.28407.

[4] K. Aldaş and R. Yapıcı, "Investigation of Effects of Scale and Surface Roughness on Efficiency of Water Jet Pumps Using CFD INVESTIGATION OF EFFECTS OF SCALE AND SURFACE ROUGHNESS ON EFFICIENCY OF WATER JET PUMPS USING CFD," no. March 2014, 2016, doi: 10.1080/19942060.2014.11015494.

[5] R. Mallela and D. Chatterjee, "Proceedings of the Institution of Mechanical Engineers , Part C : Journal of Mechanical Engineering Science," 2011, doi: 10.1177/0954406211401163.

[6] M. A. Halawa, M. A. Younes, and I. R. Teaima, "STUDY OF THE DIFFERENT PARAMETERS THAT," no. 1, pp. 1–17, 2011.

[7] G. Chen, "The effect of inlet convergence angle on flow field and performance inside the jet pump," pp. 2–4, 2011.

[8] T. Narabayashi, Y. Yamazaki, H. Kobayashi, and T. Shakouchi, "Flow analysis for single and multi-nozzle jet pump," *JSME Int. J. Ser. B Fluids Therm. Eng.*, vol. 49, no. 4, pp. 933–940, 2006.

[9] X. Long, N. Han, and Q. Chen, "Influence of nozzle exit tip thickness on the performance and flow field of jet pump †," vol. 22, pp. 1959–1965, 2008, doi: 10.1007/s12206-008-0739-4.

[10] T. A. Meakhail and I. R. Teaima, "A Study of the Effect of Nozzle Spacing and Driving Pressure on the Water Jet Pump Performance," vol. 2, no. 5, pp. 373–382, 2013.

[11] R. G. Cunningham, "Liquid jet pump modelling: effects of axial dimensions on theory-experiment agreement," in *Proceedings of the 2nd Symposium on Jet Pumps and Ejectors, BHRA Fluid Engineering, Cranfield, Bedford, UK*, 1975, vol. 24.

[12] D. F. Elger, S. J. Taylor, and C. P. Liou, "Recirculation in an annular-type jet pump," 1994.

[13] V. O. Ryzhenkov, S. S. Abdurakipov, and R. I. Mullyadzhanov, "The asymmetry of the recirculation zone of the annular jet with different diameter ratio," in *Journal of Physics: Conference Series*, 2019, vol. 1382, no. 1, p. 12035.

[14] Y. Antoine, F. Lemoine, and M. Lebouché, "Turbulent transport of a passive scalar in a round jet discharging into a co-flowing stream," *Eur. J. Mech.*, vol. 20, no. 2, pp. 275–301, 2001.

[15] L. Xiao, X. Long, X. Li, Q. Zeng, and X. Yang, "Numerical investigation on the recirculation in annular jet pumps †," vol. 27, no. 6, pp. 1603–1609, 2013, doi: 10.1007/s12206-013-0406-2.

[16] J. R. Taylor and W. Thompson, An introduction to error analysis: the study of uncertainties in physical measurements, vol. 2. Springer, 1982.

[17] H. K. Versteeg and W. Malalasekera, An introduction to computational fluid dynamics: the finite volume method. Pearson education, 2007.

[18] A. Fluent, "ANSYS fluent theory guide 15.0," *ANSYS, Canonsburg, PA*, vol. 33, 2013.

[19] F. R. Menter, R. B. Langtry, S. R. Likki, Y. B. Suzen, P. G. Huang, and S. Vö¨lker, "A correlation-based transition model using local variables: Part I—model formulation," in *Turbo Expo: Power for Land, Sea, and Air*, 2004, vol. 41693, pp. 57–67.

[20] R. B. Langtry, F. R. Menter, S. R. Likki, Y. B. Suzen, P. G. Huang, and S. Völker, "A correlation-based transition model using local variables—part II: test cases and industrial applications" Turbo Expo: Power for Land, Sea, and Air, 2006.

[21] J. C. Helton and F. J. Davis, "Latin hypercube

sampling and the propagation of uncertainty in analyses of complex systems," *Reliab. Eng. Syst. Saf.*, vol. 81, no. 1, pp. 23–69, 2003.

[22] M. D. McKay, R. J. Beckman, and W. J. Conover, "A comparison of three methods for selecting values of input variables in the analysis of output from a computer code," Technometrics, vol. 42, no. 1, pp. 55–61, 2000.

[23] N. Cressie, "The origins of kriging," Math. Geol., vol. 22, pp. 239–252, 1990.

[24] C. V Deutsch and A. G. Journel, "Geostatistical software library and user's guide," New York, vol. 119, no. 147, p. 578, 1992